Polydopamine-Decorated Microcomposites Promote Functional Recovery of an Injured Spinal Cord by Inhibiting Neuroinflammation

Wei, Guangfei

2021-10-13

Wei , G , Jiang , D , Hu , S , Yang , Z , Zhang , Z , Li , W , Cai , W & Liu , D 2021 , ' Polydopamine-Decorated Microcomposites Promote Functional Recovery of an Injured Spinal Cord by Inhibiting Neuroinflammation ' , ACS Applied Materials & Interfaces , vol. 13 , no. 40 , pp. 47341-47353 . https://doi.org/10.1021/acsami.1c11772

http://hdl.handle.net/10138/354596
https://doi.org/10.1021/acsami.1c11772

unspecified
acceptedVersion

Polydopamine-decorated Microcomposites Promote Functional Recovery of Injured Spinal Cord by Inhibiting Neuroinflammation

Guangfei Wei[a, b§], Dongdong Jiang[c§], Shuai Hu[a, b], Zhiyuan Yang[a, b], Zifan Zhang[a, b], Wei Li[d], Weihua Cai[c*], Dongfei Liu[a, b*]

[a] *State Key Laboratory of Natural Medicines, Department of Pharmaceutical Science, China Pharmaceutical University, Nanjing 210009, China*

[b] *NMPA Key Laboratory for Research and Evaluation of Pharmaceutical Preparations and Excipients, China Pharmaceutical University, Nanjing 210009, China*

[c] *Department of Orthopaedics, The First Affiliated Hospital of Nanjing Medical University, Nanjing 210029, China*

[d] *Drug Research Program, Division of Pharmaceutical Chemistry and Technology, Faculty of Pharmacy, University of Helsinki, Helsinki 00014, Finland*

* E-mail: dongfei.liu@cpu.edu.cn

* E-mail: caiwhspine@sina.com

§ *Guangfei Wei and Dongdong Jiang contributed equally to this paper*

* *Weihua Cai and Dongfei Liu are the corresponding authors of this paper*

Abstract

Neuroinflammation following spinal cord injury usually aggravates spinal cord damage. Many inflammatory cytokines are key players in neuroinflammation. Owing largely to the multiplicity of cytokine targets and the complexity of cytokine interactions, it is insufficient to suppress spinal cord damage progression by regulating only one or a few cytokines. Herein, we propose a two-pronged strategy to simultaneously capture the released cytokines and inhibit the synthesis of new ones in a broad-spectrum manner. To achieve this strategy, we designed a core/shell structured microcomposite, which was composed of a methylprednisolone-incorporated polymer inner core and a biocompatible polydopamine outer shell. Thanks to the inherent adhesive nature of polydopamine, the obtained microcomposite (MP-PLGA@PDA) efficiently neutralized the excessive cytokines in a broad-spectrum manner within one day after spinal cord injury. Meanwhile, the controlled release of immunosuppressive methylprednisolone reduced the secretion of new inflammatory cytokines. Benefiting from its efficient and broad-spectrum capability in reducing the level of cytokines, this core/shell structured microcomposite suppressed the recruitment of macrophages and protected the injured spinal cord, leading to an improved recovery of motor function. Overall, the designed microcomposite successfully achieved the two-pronged strategy in cytokine neutralization, providing an alternative approach to inhibit neuroinflammation in injured spinal cord.

Keywords

microcomposites; inflammatory cytokines; polydopamine; spinal cord injury; resolution of inflammation

Introduction

Traumatic spinal cord injury is usually caused by an initial mechanical insult to the spinal cord, such as a car accident, fall, dive or other violent events[1]. After the initial insult, nearby nerve cells and microenvironment homeostasis in spinal cord are destroyed. The initial structural and cellular damage triggers neuroinflammation, an inflammatory response within the spinal cord. This inflammatory response cleans cellular necrosis products and restores tissue homeostasis through a coordinated infiltration of immune cells (*e.g.*, microglia, neutrophils and macrophages) and release of soluble factors (*e.g.*, cytokines, chemokines and lipid byproducts)[2]. Although these efforts are essential, excessive neuroinflammation is always observed after spinal cord injury[3, 4], which usually results in the aggravation of injury, and inhibition of neuro-regeneration and functional recovery[5, 6].

During the process of trauma-induced neuroinflammation, cytokines play a central role in the initiation and regulation of inflammatory responses[1, 7-10]. The antibody to interleukin 6-receptor promotes the repair of injured spinal cord by inhibiting the excessive infiltration of hematogenous macrophages during the acute phase of spinal cord injury[11]. Neutralizing antibodies to cytokines, such as antibodies to interleukin 1α (IL-1α), tumor necrosis factor (TNF) and complement component 1, subcomponent q (C1q), successfully block A1 astrocytes production and protect injured neurons[12]. Neuroinflammation is orchestrated by a variety of cytokines, therefore, neutralization one or a few cytokines is insufficient to halt or reverse disease progression. In addition, cytokines are immediately released at the first few minutes after spinal cord injury, leading to rapid cellular infiltration and fast development of neuroinflammation[13, 14]. Therefore, alternative anti-inflammatory strategies that can rapidly modulate a variety type of inflammatory cytokines are highly desirable to inhibit neuroinflammation-induced injury and promote functional recovery.

Herein, we propose a two-pronged cytokine suppressive strategy, which can simultaneously capture the released cytokines and inhibit the secretion of new ones (**Scheme 1**). To put this strategy into practice, we engineered a core/shell structured microcomposite, MP-PLGA@PDA, which was

composed of a methylprednisolone (MP)-incorporated poly(lactic-co-glycolic acid) (PLGA) inner core (MP-PLGA) and a biocompatible polydopamine (PDA) outer shell. By displaying a PDA layer with an excellent adhesive nature, the obtained microcomposite, MP-PLGA@PDA, is expected to capture the released excessive cytokines through physical adsorption in a broad-spectrum manner[15-17]. The released MP from MP-PLGA@PDA can interfere the release of inflammatory cytokines *via* activating glucocorticoid receptors, inhibiting the expression of multiple inflammatory genes and other reducing production pathways[18, 19]. The designed MP-PLGA@PDA is anticipated to simultaneously capture the released cytokines onto the outer PDA layer and inhibit the secretion of new cytokines by the released MP (**Scheme 1**). To validate this cytokine modulation strategy, we performed cell and animal experiments to study the impact of MP-PLGA@PDA on the cytokine levels, and consequently its therapeutic outcome on a weight drop-induced spinal cord injury model.

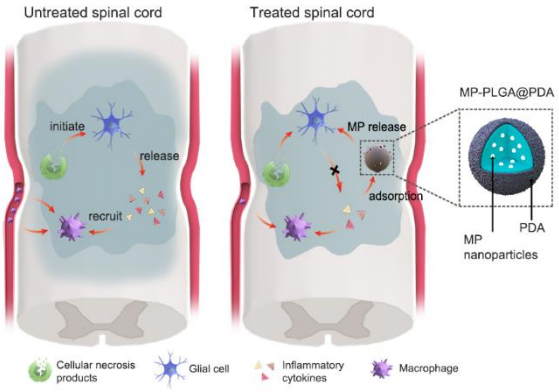

Scheme 1. A two-pronged cytokine suppressive strategy to promote functional recovery of injured spinal cord by simultaneously capturing the released cytokines and inhibiting the secretion of new ones and, consequently, inhibiting neuroinflammation.

Results and discussion

Preparation and characterization of MP-PLGA@PDA

We used a co-flow microcapillary device to engineer MP-incorporated microspheres (MP-PLGA) by an emulsion-solvent diffusion method (**Fig 1**a). The inner fluid (oil phase) was a polymer (mainly

PLGA, 10 mg/mL) dimethyl carbonate solution containing MP nanoparticles (20 mg/mL). MP nanoparticles had an average diameter of 237 nm with a polydispersity index of 0.14 (Supporting Information **Fig S1**). A poloxamer 407 solution (10 mg/mL) served as the outer fluid (water phase). Droplets grew spherically from the orifice of the inner capillary until they reached a size where the viscous drag exerted by the co-flowing outer fluid exceeded the interfacial tension (the dripping regime)[20]. Individual drops were produced periodically at the orifice of the inner glass capillary. Following the diffusion of dimethyl carbonate from droplets to the surrounding outer fluid, droplets containing PLGA and MP nanoparticles solidified, forming MP-PLGA microspheres. MP-PLGA@PDA microcomposite was engineered by simply immersing MP-PLGA in a dopamine hydrochloride solution (pH 8.5) for 24 h (**Fig 1**a).

Firstly, we characterized the obtained microcomposite by Fourier transform infrared spectroscopy (**Fig 1**b) and fluorescence microscopy (**Fig 1**c) to validate the presence of PDA layer. As shown in **Fig 1**b, three characteristic peaks at about 3300, 3400 and 1700 cm^{-1} were observed in the Fourier transform infrared spectra of MP-PLGA and MP-PLGA@PDA. Both MP-PLGA@PDA and PDA had a large and broad absorption peak from 3500 to 3200 cm^{-1}, which can be assigned to the stretching vibration of O-H, N-H, and -NH_2[21]. The Fourier transform infrared spectra indicated the presence of PDA on the surface of MP-PLGA@PDA. Fluorescein isothiocyanate (FITC) was incorporated into the PLGA matrix (FITC-PLGA) to further validate the surface decoration of PDA. We can see in **Fig 1**c, the FITC fluorescence intensity distributed evenly in FITC-PLGA microspheres before the PDA decoration. After 24 h incubation in the dopamine hydrochloride solution, FITC-PLGA was surrounded by a layer without fluorescence. The fluorescence distribution difference in FITC-PLGA and FITC-PLGA@PDA verified the successful deposition of PDA onto the surface of FITC-PLGA.

Next, we used scanning electron microscopy to characterize the obtained systems (**Fig 1**d). Both MP-PLGA and MP-PLGA@PDA (approximately 60 μm in diameter) were spherical particles with a porous structure. The pore size of MP-PLGA was larger than that of MP-PLGA@PDA (**Fig 1**d), which

could be ascribed to the surface deposition of PDA. After 24 h incubation in a dopamine hydrochloride solution, the MP loading degree declined from approximately 55.8% to approximately 39.9%; meanwhile, the PDA mass fraction increased to 28.4 ± 0.6% (**Fig 1**e). Notably, the 24 h incubation of MP-PLGA in Tris-HCl (10 mM, pH 8.5) had no effects on MP loading (Supporting Information **Fig S2**), which might be attributed to the alkaline environment (pH 8.5). Therefore, the increased mass fraction of PDA was accounted for the decrease of MP loading degree for MP-PLGA@PDA.

Then, we determined the specific surface area for both MP-PLGA and MP-PLGA@PDA by a nitrogen adsorption-desorption method. The isotherm linear plots of MP-PLGA and MP-PLGA@PDA displayed an isotherm inflection point at low relative pressure, matching the type-II adsorption-desorption behavior (Supporting Information **Fig S3**a). The correlation coefficient between the nitrogen adsorption data and Brunauer-Emmett-Teller (BET) model were higher than 0.995 (Supporting Information **Fig S3**b) and, therefore, we used the BET model to calculate specific surface area for MP-PLGA and MP-PLGA@PDA. According to the BET model[22], the specific surface area for MP-PLGA and MP-PLGA@PDA was 9.6 m^2/g and 13.2 m^2/g, respectively (**Fig 1**f). The increased specific surface area for MP-PLGA@PDA confirmed the surface deposition of PDA on MP-PLGA@PDA.

At last, we studied the *in vitro* MP release behavior for both MP-PLGA and MP-PLGA@PDA. As shown in **Fig 1**g, the complete release (approximately 94.2% MP released) was achieved within 4 h for MP group. MP-PLGA sustained the release of MP for 3 days and approximately 42.5% MP released within 4 h. In contrast, only about 26.3% MP released from MP-PLGA@PDA within 4 h; approximately 90% MP released in 3 days.

Verify the cytokine neutralization capability of MP-PLGA@PDA *in vitro*

Injury to the spinal cord causes the almost immediate release of cytokines by glial cells and neurons. To verify the cytokine neutralization capability of MP-PLGA@PDA, we first monitored the level of TNF-α, IL-6 and IL-10, after the lipopolysaccharide (LPS) stimulation on glial cells. All three

cytokines play important roles in the progress of neuroinflammation[23]. Both TNF-α and IL-6 facilitate macrophage recruitment to the injury site[24, 25]; in contrast, IL-10 decreases the secondary inflammation, excitotoxic damage, and neuronal apoptosis associated with spinal cord injury[26]. After pre-treated with LPS[27], obvious glial cells activation was observed, manifested by an upregulation of TNF-α, IL-6 and IL-10 expression (Supporting Information **Fig S5**). Subsequently, these activated glial cells were administrated with PBS, MP-PLGA, PLGA@PDA and MP-PLGA@PDA for 72 h. During the experiment period (administration from 0 to 72 h), glial cells were stimulated by LPS to continuously provide inflammatory cytokines.

As a result, the levels of these three cytokines in PBS group increased as the incubation time prolonged, and were significantly ($P < 0.05$) higher than those in the other three groups from 12 to 72 h (Supporting Information **Fig S5**). The cytokine level at each incubation time point in PBS group was used as the control. 12 h incubation of MP-PLGA with glial cells resulted in a decrease of 39.2%, 35.4% and 43.1% in TNF-α, IL-6 and IL-10, respectively. These decreases of cytokines could be attributed to the rapid release of MP from MP-PLGA. Similarly, benefiting from the excellent adhesive nature of the PDA layer[28-31], PLGA@PDA significantly ($P < 0.05$) reduced the level of TNF-α, IL-6 and IL-10 with 45.8%, 38.5% and 40.1% decreases, respectively, of the corresponding cytokine level in PBS group at 12 h after administration (**Fig 1**h). Meanwhile, the reduction of cytokines in MP-PLGA or PLGA@PDA group increased as the incubation time extended from 0 to 72 h. Until the end of this study (72 h after administration), PLGA@PDA caused a decrease of 58.8%, 45.7%, and 49.7% in TNF-α, IL-6 and IL-10, respectively.

In comparison, MP-PLGA@PDA displayed a strongest ($P < 0.05$) cytokine neutralization effect after administration for 72 h, and the cytokine level in which was only about half of that in MP-PLGA or PLGA@PDA group (Supporting Information **Fig S5**). Moreover, only 6 h after administration, MP-PLGA@PDA group had a significant ($P < 0.05$) reduction in TNF-α and IL-6, indicating its rapid cytokine neutralization effect. This rapid and highest cytokine decrease for MP-PLGA@PDA group

could be ascribed to the inherent adhesive nature of PDA towards cytokines and widespread immunosuppressive activity of MP towards the secretion of inflammatory cytokines. Thus, MP-PLGA@PDA successfully achieved the two-pronged strategy in cytokine neutralization, and demonstrated a rapid, efficient and broad-spectrum *in vitro* cytokine neutralization capability.

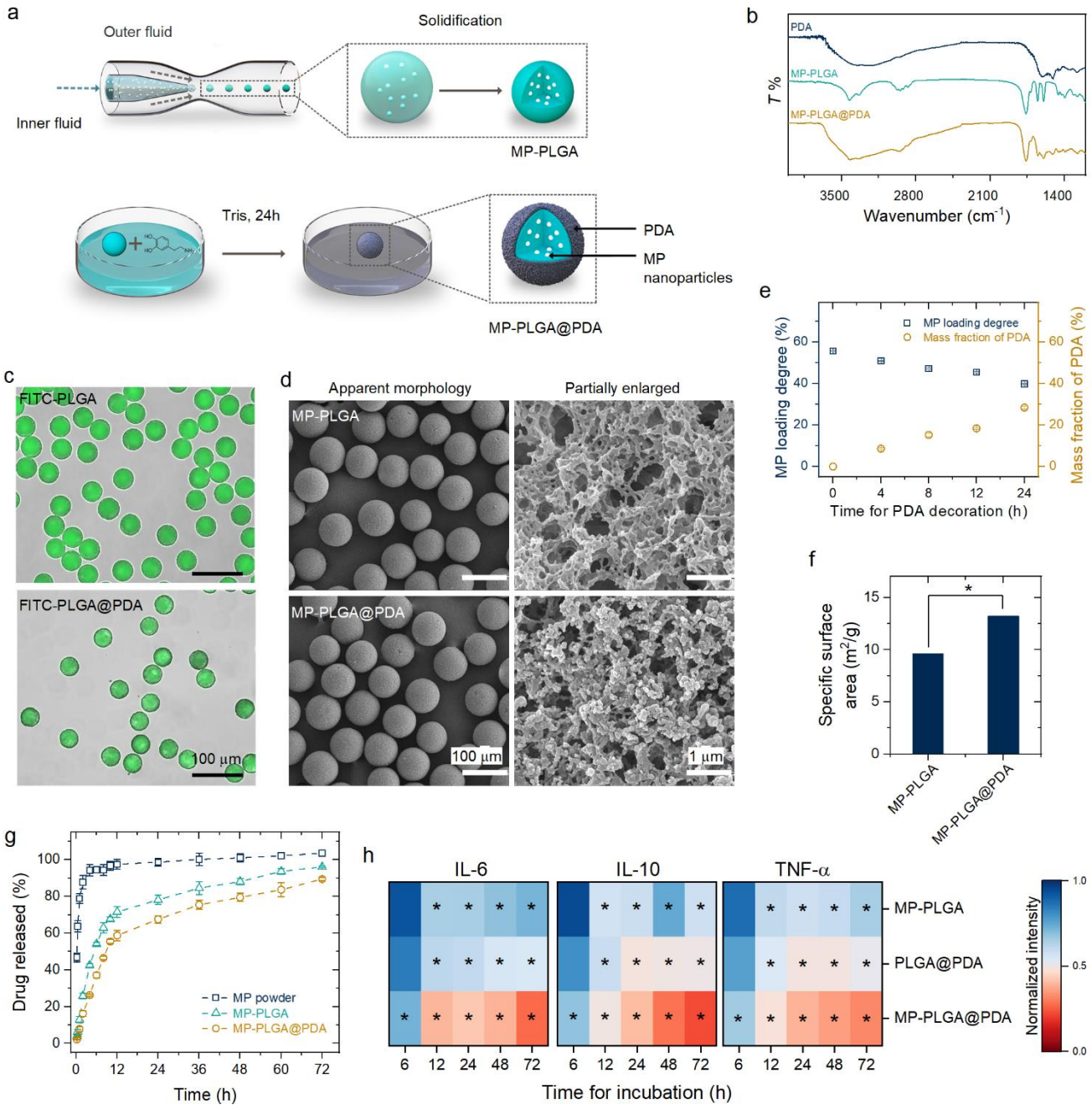

Fig 1. Preparation and characterization of MP-PLGA@PDA. (**a**) A schematic diagram of MP-PLGA@PDA preparation process. (**b**) Fourier transform infrared spectra of PDA, MP-PLGA and MP-

PLGA@PDA. (**c**) Fluorescent microscope images of FITC-PLGA before and after PDA decoration. (**d**) Scanning electron microscope images of MP-PLGA and MP-PLGA@PDA (left), and their enlarged view of the surface (right). (**e**) The effect of PDA incubation time on the MP loading degree and mass fraction of PDA. (**f**) Specific surface area of MP-PLGA and MP-PLGA@PDA calculated by BET model. (**g**) MP release profiles from MP-PLGA and MP-PLGA@PDA (n = 3). The weight of MP added to PBS for each group were equal, approximately 1 mg. (**h**) Heat map of *in vitro* cytokine inhibition effect. After stimulation with LPS (5 μg/mL) for 24 h, glial cells were treated with PBS, MP-PLGA, PLGA@PDA and MP-PLGA@PDA. The level of IL-6, TNF-α and IL-10 in culture medium was normalized by the corresponding value in PBS group at the corresponding time point (n = 6). The level of significance was set at a probability of $^{*}P < 0.05$.

MP-PLGA@PDA sustained the release of MP *in vivo*

We verified the sustained MP release capability of MP-PLGA@PDA *in vivo* at a MP dose of 400 μg (**Fig 2**a). MP concentration in cerebrospinal fluid as a function of time was analyzed by a liquid chromatography coupled with a triple quadrupole mass spectrometry. For MP group, the drug concentration reached a peak (C_{max}, about 33.7 μg/mL) at 6 h after administration and rapidly declined to about 1.9 μg/mL within 1 day with a $t_{1/2}$ value of 5.7 h (**Fig 2**b). In comparison with MP group, a relatively lower C_{max} (about 11.3 μg/mL) for MP-PLGA@PDA group was observed, and the $t_{1/2}$ was prolonged to 28.8 h. Similarly, MP-PLGA group reached the peak concentration (C_{max}, about 11.1 μg/mL) at 6 h after administration with a $t_{1/2}$ of 25.5 h.

We also calculated the area under the concentration-time curve (AUC, **Fig 2**c) and the mean residence time (MRT, **Fig 2**d) of MP in cerebrospinal fluid. The AUC and MRT of MP for MP group were 168.7 ± 29.9 μg/mL·h and 7.6 ± 0.2 h, respectively. In comparison with MP group, a larger AUC and a longer MRT were observed in MP-PLGA group (313.3 ± 17.6 μg/mL·h; 27.5 ± 1.4 h) and MP-PLGA@PDA group (305.5 ±16.9 μg/mL·h; 26.6 ± 0.8 h), indicating the sustained MP release from microspheres. In addition, for MP-PLGA and MP-PLGA@PDA, there was no significant difference

on the AUC and the MRT of MP, suggesting that the deposition of PDA had no significant effect on the MP pharmacokinetic profile ($P > 0.05$).

In vivo broad-spectrum cytokine neutralization by MP-PLGA@PDA

We inspected the cytokine neutralization capability of MP-PLGA@PDA on a rat with a weight-drop injured thoracic spinal cord. Within one day post-injury, all 23 tested inflammatory cytokines were upregulated, which could lead to fast cellular infiltration and inflammatory development[13, 14]. In comparison with Saline group, MP-PLGA significantly reduced the level of all 23 tested cytokines except IL-13, granulocyte-macrophage colony-stimulating factor (GM-CSF) and TNF-α, at day 1 post-injury (**Fig 2**e). Unfortunately, at day 3 post-injury, the cytokine modulation effect of MP-PLGA was only observed on 9 cytokines (IL-1α, IL-1β, IL-6, IL-18, GRO/KC, MCP-1, MIP-1α, MIP-3α and RANTES). When came to day 7 post-injury, there was no significant difference ($P > 0.05$) on the level of all 23 tested cytokines between MP-PLGA group and Saline group, except IL-1α, IL-1β and IL-6. This reduced cytokine modulation of MP-PLGA could be ascribed to the immunosuppressive feature of the released MP molecules, which was approximately 5.0 μg/mL in cerebrospinal fluid at one day post-injury, but only about 1.3 μg/mL at day 3 post-injury, and negligible level of MP at day 7 post-injury (**Fig 2**b).

Similarly, PLGA@PDA significantly (comparing with Saline group, $P < 0.05$) reduced the level of all 23 tested cytokines within one day post-injury (**Fig 2**e), displaying their fast and broad-spectrum adsorption nature toward cytokines. This efficient cytokine modulation capability was consistent with previous studies that dopamine-decorated materials efficiently have captured albumin within 30 min[28]. At day 3 post-injury, the cytokine modulation effect by PLGA@PDA was still observed on all 23 tested cytokines, except IL-4, IL-12, IL-13, granulocyte colony stimulating factor (G-CSF), GM-CSF, TNF-α, and vascular endothelial growth factor (VEGF). As the injury in spinal cord progresses, the surface of PLGA@PDA adsorbed a quantity of cytokines, thus, the driving force (concentration of cytokines gradient) for physical adsorption went downhill. And the cytokine modulation effect of

PLGA@PDA was only observed on 5 cytokines (IL-1α, IL-1β, IL-2, IL-6, and GM-CSF) at day 7 post-injury. Therefore, the rapid and broad-spectrum cytokines adsorption feature of PDA was mainly displayed in the early stage of neuroinflammation.

MP-PLGA@PDA was anticipated to merge the adhesive feature of PDA by capturing released cytokines and widespread immunosuppressive activity of MP by reducing inflammatory cytokine release. Satisfyingly, after the administration of MP-PLGA@PDA for only one day, TNF-α, IL-6 and IL-1β were found for over 80% decrease when comparing with the Saline group (**Fig 2**e). Most importantly, the increase of all the tested 23 cytokines was blunted, demonstrating the broad-spectrum cytokine neutralization capability for MP-PLGA@PDA. This broad-spectrum cytokine modulation capability is expected to efficiently attenuate the neuroinflammation after spinal cord injury. It should also be noted that some anti-inflammatory cytokines, like IL-4, IL-10 and IL-13, were undesirably but unavoidably reduced at day 1 post-injury, which might be attributed to this unselective cytokine neutralization of MP and PDA[32]. Comfortingly, the reduction of anti-inflammatory cytokines was mainly found at day 1 post-injury. In addition, the level of vascular endothelial growth factor (VEGF) at day 7 post-injury for all three groups was significantly upregulated, compared with that at day 1 post-injury.

We performed molecular dynamics simulations to probe the mechanisms of PDA material-cytokine interactions in atomistic detail, especially the driving force towards the broad-spectrum cytokine neutralization capability of PDA. Due to its high degree of disorder at all structural levels, the molecular structures of PDA are still unclear to date[33]. It is a challenge to simulate the formation of PDA layer, therefore, a dopamine tetramer, a most stable molecular structure of polydopamine [33], was selected to perform the simulations. The interaction energy between cytokines and the dopamine tetramer, including the Lennard-Jones and Coulomb interactions, was calculated (**Fig 2**f). When interacting with a dopamine tetramer the lowest Lennard-Jones interaction energy value was observed on IL-18 (-21.4 ± 21.5 KJ/mol) among all the 23 tested cytokines, and IFN-γ showed the highest value

(-121.5 ± 15.6 KJ/mol). The Coulomb interaction energy varied from -883.3 ± 70.9 KJ/mol (IL-12) to -225.7 ± 65.3 KJ/mol (IL-2). Among 23 tested inflammatory cytokines, their interaction with the dopamine tetramer all showed negative values for both the Coulmb interaction energy and the Lennard-Jones interaction energy. These negative values suggested the broad-spectrum cytokine neutralization capability for PDA. Regarding the interaction between cytokines and the dopamine tetramer, the Coulmb interaction energy was always stronger than the corresponding Lennard-Jones interaction energy.

Next, we assessed the types and number of amino acid residues involved in the interaction with the dopamine tetramer. The hydrogen bond and hydrophobic interaction were analyzed by the LigPlot^{+}. Taking the G-CSF as an example (**Fig 2**g), Asp 21 and Glu 27 (green residues) involved in hydrogen bond interactions; Glu 13, Lys 17, Arg 16, Gly 20 and Ala23 (black residues) involved in the hydrophobic interactions (eyelash-like marks). Regarding the hydrogen bond acceptors and donors on the dopamine tetramer, cytokines and the dopamine tetramer have strong Coulomb interactions. It is consistent with molecular dynamics simulation results of interaction energy that the Coulomb force made the primary contribution in the adsorption process.

We further analyzed the occurrence frequency of amino acid residues involved in hydrogen bond (**Fig 2**h) and hydrophobic interaction (**Fig 2**i) between different kinds of cytokines and the dopamine tetramer. As shown in **Fig 2**h, the hydrogen bond interaction mainly came from the Asp and Glu residues within inflammatory cytokines, which showed high frequency of occurrence. Hydrophobic interaction is a kind of property of nonpolar molecules, which can drive these molecules to assemble to form anhydrous domains in aqueous solution. Hydrophobic interactions are important for the folding of proteins and widely exists among amino acid residues. As expected, there was no significant difference in the frequency among different kinds of amino acid residues in hydrophobic interactions (**Fig 2**i).

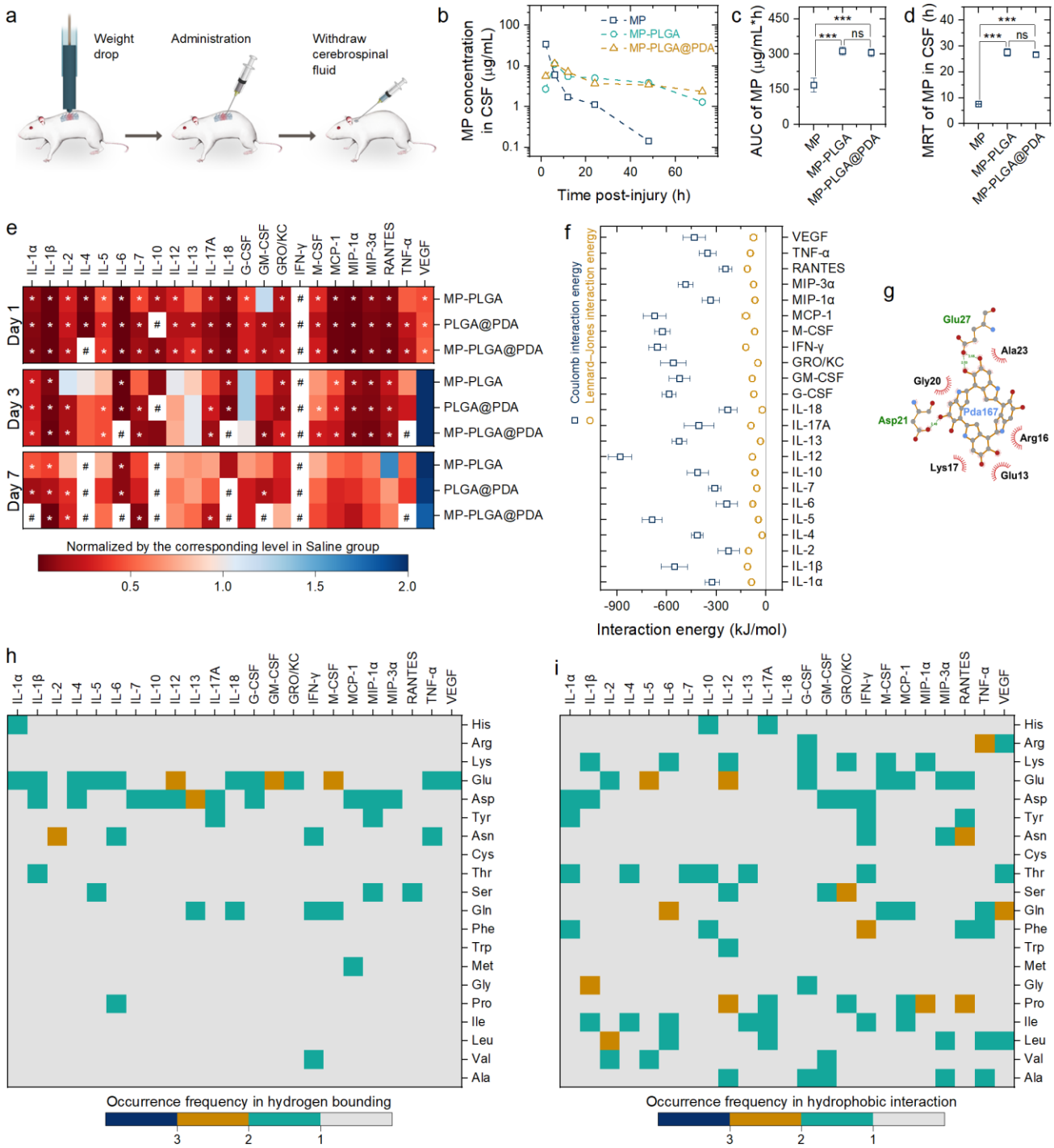

Fig 2. The inflammatory cytokines neutralization capability of MP-PLGA@PDA. (**a**) Schematic diagram of experimental design. Formulations were intrathecally injected in a rat model with a weight-drop injured thoracic spinal cord. (**b-d**) Pharmacokinetic study. Concentration-time curves (**b**) of MP in cerebrospinal fluid (CSF) after intrathecal injection of MP, MP-PLGA and MP-PLGA@PDA in rats after spinal cord injury, the corresponding area under curve (AUC; **c**) and mean residence time (MRT;

d). Every rat was only sampled once; $n = 6$ at each time point for each group. The Saline group served as the control; ns, not significant; $^{***}P < 0.001$. (**e**) Heat map of inflammatory cytokines in cerebrospinal fluid ($n = 3$). Cerebrospinal fluid was collected at day 1, 3 and 7 post-injury to quantify inflammatory cytokines. The level of cytokine was normalized by its corresponding value in Saline group at the corresponding time point. Saline group served as the control; $^{*}P < 0.05$; #, lower than the limit of detection. G-CSF, granulocyte colony stimulating factor; GM-CSF, granulocyte-macrophage colony-stimulating factor; GRO/KC, growth-related oncogene/keratinocyte chemoattractant; IFN-γ, interferon-γ; MCP-1, monocyte chemoattractant protein-1; MIP, macrophage inflammatory protein; VEGF, vascular endothelial growth factor. (**f**) The Lennard-Jones and Coulomb interaction energy between different kinds of cytokines and the dopamine tetramer. (**g**) The Ligplot analysis diagram of the dopamine tetramer which was interacting with G-CSF. Red spheres, oxygen atoms; blue spheres, nitrogen atoms; and gray spheres, carbon atoms. The green residues (Asp 21 and Glu 27) involve in hydrogen bond interaction. The black residues (Glu 13, Lys 17, Arg 16, Gly 20 and Ala23) involve in the hydrophobic interaction. The eyelash-like marks mean hydrophobic interaction. (**h** and **i**) Occurrence frequency of amino acid residues involved in hydrogen bond (h) and hydrophobic interaction (i) between different kinds of cytokines and the dopamine tetramer.

MP-PLGA@PDA inhibited macrophage recruitment and protected neurons

Activated microglia can respond within minutes after injury with production of pro-inflammatory cytokines[34]. These inflammatory cytokines can promote the influx of hematogenous macrophages from the circulation. The recruited macrophages and activated microglia usually aggravate the secondary damage toward the injured spinal cord[1, 8-10, 35]. To study the outcome of cytokine reduction by MP-PLGA@PDA, we collected the injured spinal cord and evaluated the level of macrophages and activated microglia at the injury site (**Fig 3**a and b). The border of injury site was identified by immunostaining of glial fibrillary acidic protein (GFAP; in green). Recruited macrophages and activated microglia were identified by F4/80 (in red)[36], and the fraction of these F4/80-positive cells

in the injury site was qualified by Volumetric Tissue Exploration and Analysis (VTEA)[37] (**Fig 3**c and d). At day 3 post-injury, the F4/80 intensity in the damage area was the brightest for Saline group with a highest fraction of F4/80-positive cells in injury site (approximately 5.5%). In comparison with Saline group, the administration of MP-PLGA, PLGA@PDA, MP-PLGA@PDA significantly ($P < 0.001$) reduced the fraction of F4/80-positive cells to about 3.6%, 3.3% and 1.7%, respectively. Moreover, the level of F4/80-positive cells in MP-PLGA@PDA group was significantly ($P < 0.001$) lower than that in MP-PLGA group and PLGA@PDA group, indicating the macrophage recruitment inhibition of MP-PLGA@PDA.

We further examined the level of edema in spinal cord at day-3 post injury by a magnetic resonance imaging unit (**Fig 3**e). The edema volume, recognized by hyperintense signal in T2 weighted images, was illustrated in **Fig 3**f. At day 3 post-injury, the edema volume for MP-PLGA@PDA group (approximately 2.2 mm^3) was only 33.3% of that in Saline group (approximately 6.6 mm^3), 45.8% of that in MP-PLGA group (approximately 4.8 mm^3), and 50.3% of that in PLGA@PDA group (approximately 4.3 mm^3). As expected, MP-PLGA@PDA group significantly reduced the volume of edema.

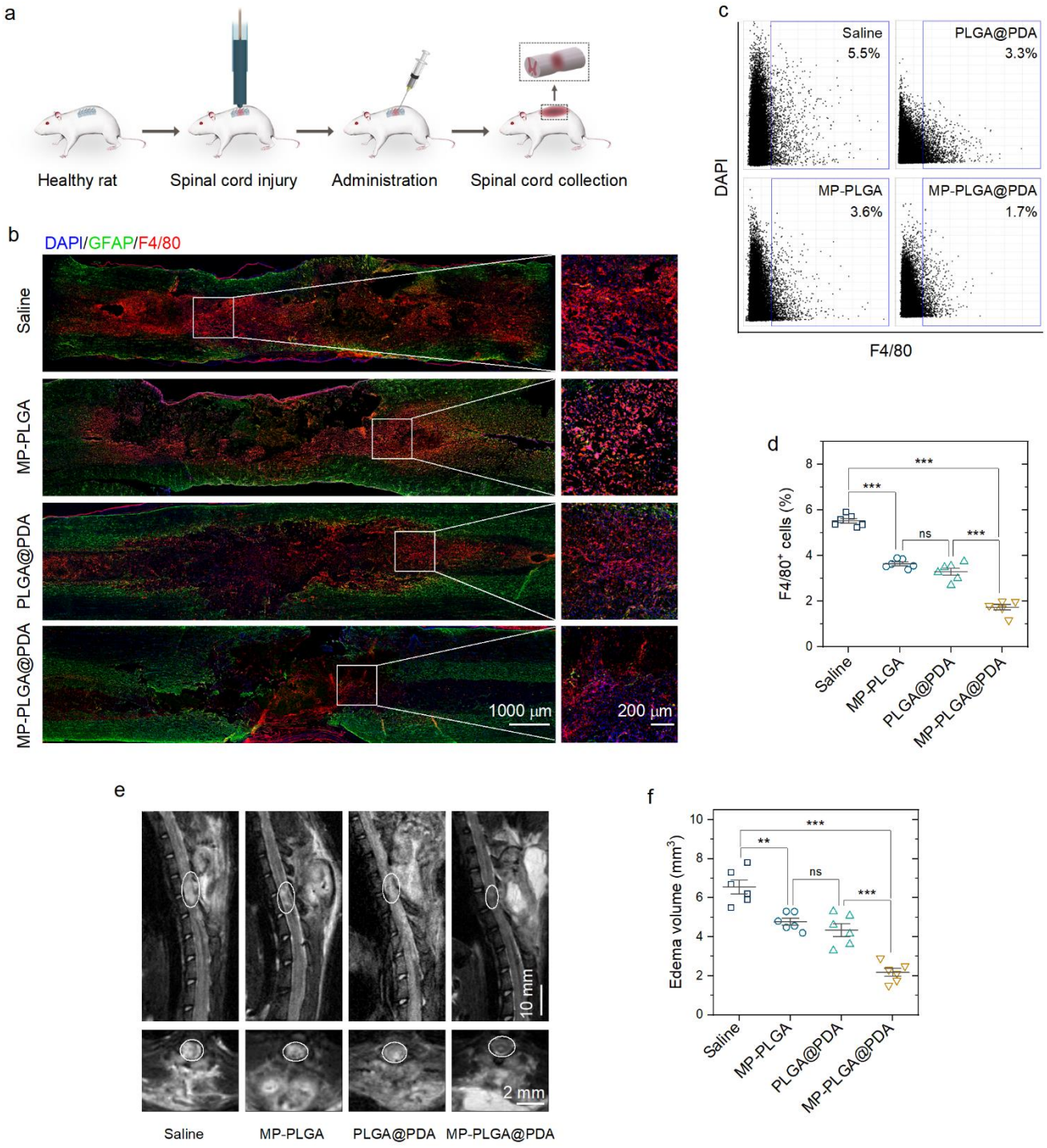

Fig 3. MP-PLGA@PDA inhibited the recruitment of macrophages after spinal cord injury. (**a**) Schematic diagram of experimental procedure. (**b**) Representative images of immunofluorescence staining for damaged area (GFAP, in green) and macrophages (F4/80, in red) in longitudinal sections of injured spinal cord at day-3 post-injury. The nuclei of all cells were stained with DAPI (in blue). (**c**) Representative scatterplots showing F4/80 versus DAPI from VTEA analysis of the image volumes.

A gate was drawn to identify cells with high F4/80 immunofluorescence. (**d**) Summary of results obtained from VTEA analysis comparing the effect of MP-PLGA@PDA on the percentage of F4/80-positive cells ($n = 6$). (e) Sagittal and axial spinal cord T2 weighted magnetic resonance images at day-3 after injury. (**f**) Edema volume obtained from magnetic resonance images ($n = 6$). ns, not significant; $^{**}P < 0.01$; $^{***}P < 0.001$.

The density and status of neurons play an important role in the outcome of injured spinal cord after the initial mechanical insult. The 200kDa subunit of a neurofilament (NF200) is qualified as potential surrogate markers of damage to neuron and axon[38]. Therefore, we further examined the density or status of axons in the injured spinal cord by immunostaining NF200 to verify the therapeutic outcome of cytokine modulation strategy (**Fig 4**). In all groups, the NF200 intensity near the peritraumatic area was lower than that located further from the traumatic lesion, indicating neurons damage occurred. The decrease of NF200 intensity was qualified by the intensity in regions near lesion and that in regions located >10 mm from the border of the injury (**Fig 4**b and **Fig S**6). At day 28 post-injury, the NF200 intensity in Saline group decreased for approximately 56.3% when comparing with that in regions located >10 mm from the border of the injury. In comparison with Saline group, the decrease of NF200 intensity was significantly reduced to 38.2% ($P < 0.001$), 39.1% ($P < 0.001$) and 21.5% ($P < 0.001$) for MP-PLGA, PLGA@PDA and MP-PLGA@PDA, respectively (**Fig 4**c). Moreover, the decrease of NF200 intensity in MP-PLGA@PDA group was significantly smaller than that in MP-PLGA group ($P < 0.001$) and PLGA@PDA group ($P < 0.001$).

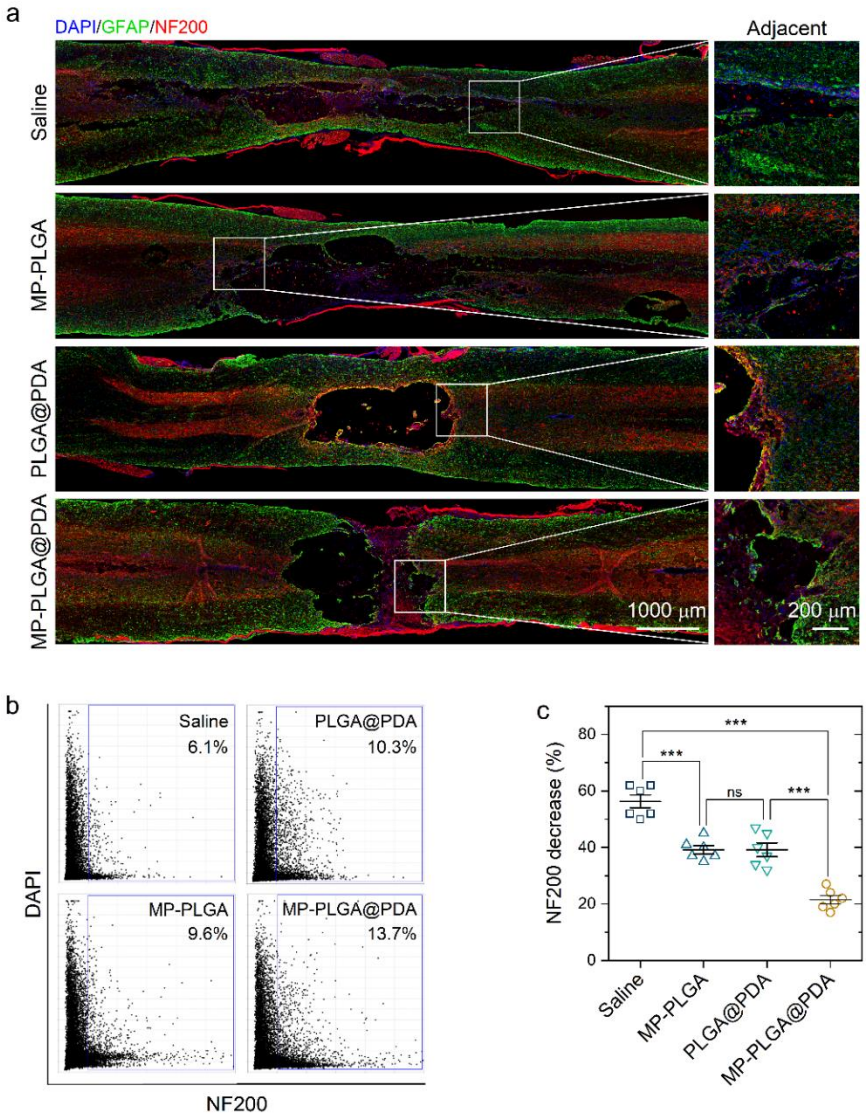

Fig 4. Neuroprotection of MP-PLGA@PDA towards the injured spinal cord. (**a**) Representative immunohistochemical staining images of GFAP (in green) and NF200 (in red) in longitudinal sections of injured spinal cord at day-28 post-trauma. The nuclei of all cells were stained with DAPI (in blue). The right columns are the enlarged images corresponding to the area adjacent to the lesion. (**b**) In regions adjacent to lesion, cells were identified, and their average DAPI versus the average NF200 intensity was plotted from VTEA analysis. A gate was drawn identifying cells with high NF200 immunofluorescence. (**c**) Semi-quantification the effect of MP-PLGA@PDA on the intensity decreases of NF200. The data are plotted as the relative value of NF200 intensity near the injury site compared with that in distant area (n = 6). ns, not significant; $^{***}P < 0.001$.

Neuroinflammation is an important factor of spinal cord injury, and alleviating neuroinflammation is believed to reduce disease severity and improve patient outcome in most cases. In the secondary tissue damage in injury to spinal cord, a variety of cytokines orchestrate the progress of neuroinflammation. Benefiting from its rapid, efficient and broad-spectrum cytokine neutralization capability, MP-PLGA@PDA efficiently reduced 21 types of cytokines out of all 23 tested ones within one day after spinal cord injury. The efficient neutralization of cytokines after spinal cord injury enabled MP-PLGA@PDA to reduce the level of macrophages at the injury site, to relieve the edema in spinal cord, and to protect the neurons and axons at the injury site in spinal cord. Therefore, MP-PLGA@PDA neutralized cytokines in a broad-spectrum manner, which inhibited the progression of neuroinflammation-induced injury.

MP-PLGA@PDA improved motor function recovery

Finally, we moved to the motor function recovery test to evaluate the therapeutic outcome of MP-PLGA@PDA. The motor behavior in open-field was assessed by the 21-point Basso, Beattie, and Bresnahan (BBB) locomotor rating scale. As a result of spinal cord injury, rats in all groups lost their hindlimb motor function (BBB score = 0) at day 1 post-injury (**Fig 5**a). At day 28 post-injury, the dexterity of hindlimbs for rats in MP-PLGA@PDA group (BBB score = 13.7 ±1.5) was significantly higher ($p < 0.05$) than that for rats treated with Saline (BBB score = 6.7 ± 0.6), MP-PLGA (BBB score = 9.7 ± 1.1) and PLGA@PDA (BBB score = 10.0 ± 1.0). In comparison with MP-PLGA and PLGA@PDA, a faster rising trend in the BBB scores was observed for rats treated with MP-PLGA@PDA.

We further analyzed the footprints of rats to assess the locomotor activity of hindpaws at day 28 post-injury (**Fig 5**b). The stride length of footprints in Saline group was significantly shorter than that in PLGA@PDA group and MP-PLGA group (**Fig 5**c and **5**d, $P < 0.05$). MP-PLGA@PDA group showed the highest improvement in stride length. Quantitatively, MP-PLGA@PDA induced a nearly 1.3-fold increase in the co-ordination of forepaw-hindpaw movements with a stride length of 13.8 ±

0.8 cm, compared with MP-PLGA and PLGA@PDA, whose stride length was 10.6 ± 1.3 cm and 10.1 ±1.1 cm, respectively. Rats in MP-PLGA@PDA group revealed frequent to consistent weight supported plantar steps and occasional forelimb-hindlimb coordination. The motor-evoked potential assay provided further evidence on the most obvious recovery in MP-PLGA@PDA group (**Fig 5**e and f). Specifically, MP-PLGA@PDA group exhibited the highest motor-evoked potential amplitudes (70.2 ± 2.8 mv). No significant difference on the motor-evoked potential amplitudes was observed for MP-PLGA (approximately 61.3 mv) and PLGA@PDA (approximately 61.7 mv). The motor-evoked potential assay revealed that MP-PLGA@PDA had improved the recovery of electrophysiological functions for hindlimbs.

All three motor function assays showed that MP-PLGA@PDA treated rats significantly enhanced recovery of hindlimb motor function. Neutralization of broad-spectrum cytokines by MP-PLGA@PDA, not only could inhibit neuroinflammation-induced injury, but also could further enable the functional recovery of axonal network in the injured lesion area.

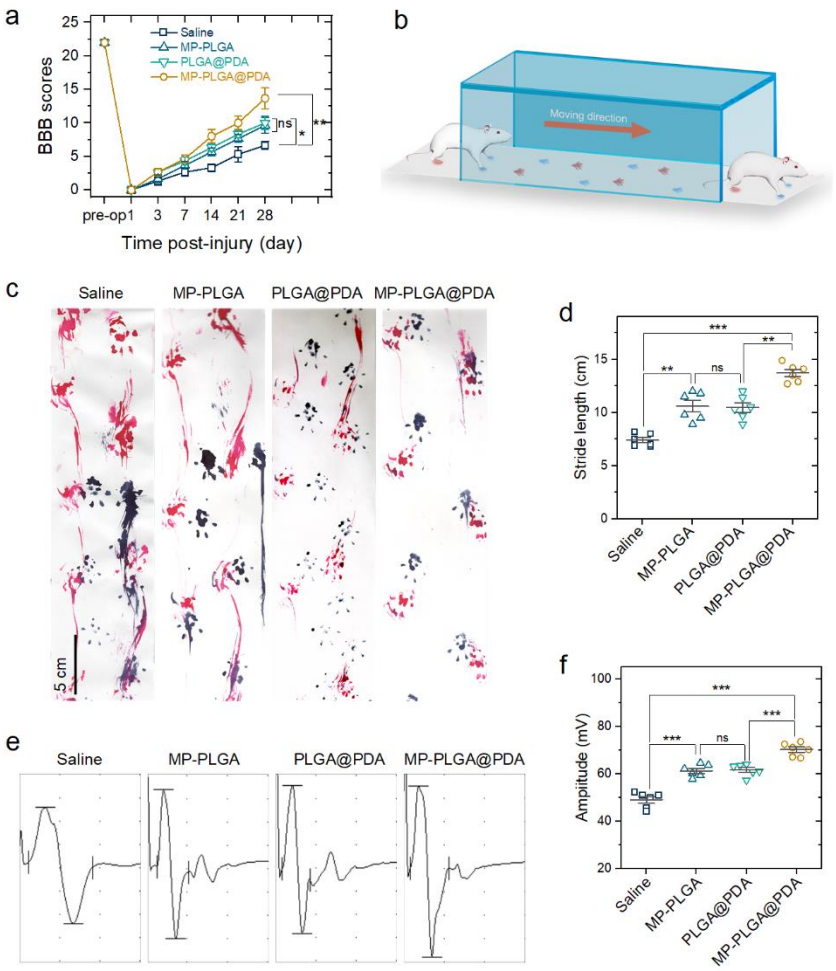

Fig 5. MP-PLGA@PDA promoted the recovery of motor function. (**a**) The rats were functionally graded up to 28 days post-injury by BBB grading scale. The BBB scores in these four groups were analyzed at day 28 post-injury. (**b**) Schematics of the motor function test. (**c** and **d**) Representative footprint images (c) and quantification of stride length (d) of rats treated with different formulations at day 28 post-injury. Blue, forepaw print; red, hindpaw print. (**e**) Representative motor evoked potentials of spinal cord injured rats treated with different formulations. The nerve conduction function of hindlimb was monitored by amplitude under a single square wave stimulus (0.5 mA, 0.5 ms, 1 Hz). (**f**) Quantitative analysis of the amplitude of motor evoked potentials ($n = 6$). ns, not significant; $^{*}P < 0.05$; $^{**}P < 0.01$; $^{***}P < 0.001$.

Conclusion

We have engineered a core/shell microcompoiste, MP-PLGA@PDA, and demonstrated their neuroinflammation inhibition potential for spinal cord injury therapy. Our microcomposite successfully realized the proposed two-pronged cytokine suppressive strategy, which could simultaneously capture the released cytokines in a broad-spectrum manner by the outer PDA surface and inhibit the synthesis of new cytokines with the help of immunosuppressive methylprednisolone. Unlike existing anti-cytokine agents that inhibit specific targets, our microcompoiste (MP-PLGA@PDA) provids a broad-spectrum blockade that dampens the inflammation cascade in spinal cord injury. In addition, the surface decorated PDA layer allows the core-shell structured microcomposite to neutralize relevant inflammatory cytokines without the need to identify them. As a result, MP-PLGA@PDA efficiently reduces excessive neuroinflammation, inhibits neuroinflammation-induced injury and promotes functional recovery of spinal cord injury.

Materials and methods

Engineering of MP-PLGA and MP-PLGA@PDA

The co-flow microfluidic devices were assembled by borosilicate glass cylindrical capillaries and microscope slides, as described previously[39]. MP-PLGA microspheres were prepared by the emulsion-solvent diffusion method. Methylprednisolone nanoparticles were prepared by ball milling at 1200 rpm for 1 h in PLGA dimethyl carbonate solution. The inner fluid was polymer (10 mg/mL; mainly PLGA 502H, Sigma-Aldrich, USA) dimethyl carbonate solution containing methylprednisolone nanoparticles (20 mg/mL; TCI, Japan). A poloxamer 407 (BASF, Germany) solution (1%, w/v; pH 8.0) served as the outer fluid. Subsequently, the inner fluid (0.8 mL/h) and outer fluid (15 mL/h) were pumped into a co-flow microfluidic device using pumps (PHD Ultra, Harvard Apparatus, USA), which flowed in the same direction. When the inner and outer fluids met, oil-in-water emulsion droplets were generated under the shear stress of the outer fluid. Following the diffusion of dimethyl carbonate from

droplets to the surrounding outer fluid, the formed oil-in-water emulsion were solidified and MP-PLGA microspheres were prepared. Fluorescein isothiocyanate (FITC; 1 mg/mL; Aladdin, China) was added into PLGA (10 mg/mL) dimethyl carbonate solution to prepared FITC-PLGA.

PDA decorated microcomposites were prepared by simply immersing MP-PLGA or FITC-PLGA in dopamine hydrochloride solution (pH 8.5), according to a method previously reported[40]. Briefly, after dissolving dopamine hydrochloride (100 mg, Aladdin, China) in Tris buffer (10 mL, 10 mM, pH 8.5), MP-PLGA (15 mg) was added into dopamine solution under mild stirring at room temperature for 24 h. After washing with dd-water for three times, MP-PLGA@PDA or FITC-PLGA@PDA was obtained.

Characterization of MP-PLGA@PDA

The decoration of PDA on the surface of microcomposites was analyzed by Fourier transform infrared spectroscopy (Vertex 70, Bruker, USA). The Fourier transform infrared spectra were recorded at room temperature between 4000-1200 cm^{-1} with a resolution of 4 cm^{-1}. The fluorescence intensity of FITC-PLGA and FITC-PLGA@PDA were observed in bright and FITC channels using a fluorescence microscope (Observe 7, ZEISS, Germany). The surface morphology of obtained microcomposites was further studied by scanning electron microscopy (Sigma 500, ZEISS, Germany).

Nitrogen adsorption-desorption

The specific surface area was analyzed by nitrogen adsorption-desorption method (ASAP3020, Micromeritics, USA). After pressurization and decompression, the isotherm linear plots were obtained under the analysis bath temperature of 77.35 k. The adsorption-desorption behavior was analyzed by the Brunauer-Emmett-Teller (BET) theory[41].

Drug loading and *in vitro* drug release

The loading degree for MP-PLGA and MP-PLGA@PDA, expressed as [(weight of loaded drug/weight

of drug loaded samples) × 100%], was determined by immersing them into dimethyl sulfoxide to dissolve all MP and PLGA matrix. To estimate the sustained release performance of microcomposites, MP-PLGA, MP-PLGA@PDA and MP were immersed in 50 mL PBS (pH 7.4) at 37 °C with shaking at 100 rpm. The weight of MP added to PBS for each group were equal, approximately 1 mg. At various specified time, 200 μL medium was taken and replaced with 200 μL fresh medium. The cumulative release percentage of MP in each group was defined as [(cumulative mass of released MP at a certain time/the initial mass of MP added to PBS samples) × 100%]. The concentration of MP in PBS or dimethyl sulfoxide was analyzed by a high-performance liquid chromatography equipped with a photo-diode-array detector (LC-20AD, Shimadzu, Japan) and a column of C18 column (Kromasil ®, 5mm, 150 × 4.6 mm). The mobile phase, composed of 58% (v/v) acetic acid (0.5%, pH 3) and 42% (v/v) acetonitrile, was set at a flow rate of 1 mL/min. The detection wavelength was 245 nm.

Verify the cytokine neutralization capability *in vitro*

The cytokine neutralization capability of MP-PLGA@PDA was evaluated on primary glial cells. Glial cells were purified and cultured in 24-well plates, as described previously[42]. This experiment was approved by the animal ethics committee of China Pharmaceutical University (202103003). After stimulation with lipopolysaccharide (LPS, 5 μg/mL) for 24 h, these glial cells were treated with PBS, MP-PLGA, PLGA@PDA and MP-PLGA@PDA. Regarding MP-PLGA and MP-PLGA@PDA, the final concentration of MP was fixed at 180 μg/mL; the corresponding amount of bare PLGA@PDA microspheres was used. At the given time point, the level of IL-6, TNF-α and IL-10 in culture medium was measured of using ELISA kits (Multi Sciences, China), according to the manufacturers' protocol.

Animal model for spinal cord injury and administration of formulations

All care and handling of animals were performed according to the international laws and policies (EEC Council Directive 86/609, 1987) and approved by the animal ethics committee of China Pharmaceutical University (202103003). Care of animals was done within institutional animal-care

committee guidelines. Sprague-Dawley rats (8 weeks old) were used to establish the spinal cord injury model. Under general anesthetic (chloral hydrate, 350 mg/kg body weight) and sterile conditions, a T10 laminectomy was performed to expose the underlying thoracic spinal cord segment. Next, spinal cord contusion injury was produced using a weight-drop device (RWD Life Science Corp., C4P01-001, China). The volume for all the formulations was 10 μL. The MP dose was 400 μg for MP-PLGA and MP-PLGA@PDA. The amount of PLGA@PDA used was equal to the corresponding matrix in MP-PLGA@PDA.

Pharmacokinetic study

Formulations were intrathecally administrated at MP dose of 400 μg/10 μL[43]. Cerebrospinal fluid was collected by a syringe (1 mL) equipped with a 25G disposable needle (0.5 mm × 20 mm), as described previously[44, 45]. The volume of cerebrospinal fluid samples ranged between 100 and 150 μL. Cerebrospinal fluid samples were mixed with 50% ethanol-water at the equivalent volume and 200 μL internal standard solution (100 ng/mL tolbutamide). Then, the mixtures were vortexed for 3 min, and centrifuged for 5 minutes at 18000 g. An aliquot of 1 μL supernatant was injected for LC-MS/MS (Waters Technologies-TQ6500, Triple quad, CA, USA) analysis with a polar C18 column (Luna ®, Omega, 1.6 μm, 50 × 2.1 mm). The mobile phase was a mixture of acetonitrile and water (0.1% formic acid added respectively) at a flow rate of 0.6 mL/min. Mass spectrometric detection was carried out under electrospray (ESI) positive ion modes and using triple quadrupole mass spectrometer. Multiple reaction monitoring (MRM) was used to monitor the transition of the deprotonated molecule *m*/*z* of 375.1 to the product ion 185 for MP.

Cytokine level in cerebrospinal fluid

The concentration of cytokines in cerebrospinal fluid was monitored using a Luminex liquid suspension chip, which was performed by Wayen Biotechnologies (Shanghai, China). The Bio-Plex Pro Rat Panel 23-plex Cytokine kit was used in accordance with the manufacturer's instructions. In

brief, cerebrospinal fluid was added into plates embedded with microbeads and incubated for 1 h. After that, the corresponding antibody was added into wells and incubated for 0.5 h. Then, streptavidin-PE was added into each well. After 10 min incubation, the signal in each well was measured by a Bio-Plex MAGPIX System (Bio-Rad; California, USA).

Molecular dynamics simulation of the interaction between cytokines and dopmaine

The interaction between all 23 tested inflammatory cytokines and a cyclic dopamine tetramer was evaluated in all-atom molecular dynamics simulations. The starting 3D structures of inflammatory cytokines were obtained from the Protein Data Bank with entry codes of 5ZO6 (GCSF), 5D22 (GMCSF), 1MSH (GRO/KC), 1FYH (IFN-γ), 2KKI (IL-1α), 1T4Q (IL-1β), 4NEJ (IL-2), 2B8Z (IL-4), 3B5K (IL-5), 1ALU (IL-6), 3DI2 (IL-7), 2H24 (IL-10), 1F45 (IL-12), 3LB6 (IL-13), 4HR9 (IL-17 α), 3F62 (IL-18), 1DON (MCP-1), 5LXF (M-CSF), 2X69 (MIP-1 α), 2JYO (MIP-3 α), 1RTO (RANTES), 2AZ5 (TNF-α), and 1WQ9 (VEGF). In molecular dynamics simulations, the cyclic dopamine tetramer, a most stable molecular structure of polydopamine[33], was selected to represent the crosslinked structure of polydopamine. At first, one cytokine and one dopamine tetramer were placed randomly in a cubic box with a minimum distance of 1.5 nm between any heavy atom of solute and box. Then, the simulation box was solvated with plenty of water molecules, and finally, Na^+ or Cl^- ions were added to neutralize the system. The all-atom molecular dynamics simulations were performed by using the Gromacs 2019.6 package with Gromos 54a7 force field. The SPC water model was chosen. The particle mesh PME method was used to calculate the long-range electrostatic interaction, whereas the Lennard-Jones interaction was treated with a cut-off distance of 1.4 nm. LINCS was applied to constrain the hydrogen bond within the protein. Periodic boundary conditions were applied in all three directions. The energy minimization was firstly performed for about 50,000 steps. After energy minimization, the system with the protein and the polydopamine monomer positionally restrained was equilibrated for 1 ns at a constant pressure of 1 bar and a temperature of 298 K with Berendsen coupling methods. Then, the restriction of the protein and the polydopamine monomer was turned off, and the

system was performed in the NVT ensemble at 298 K for 50 ns. The integration time step was 1 fs.

Motor function analysis

To examine the therapeutic outcome, the motor function of spinal cord injured rats was evaluated by BBB scoring method, footprint test and electrophysiology analysis. The BBB locomotor score was assessed by two independent examiners blinded to the treatment formulations. The motor functions including the hind-limb joint activities, motion range, load-bearing capacity, coordination of limbs, and movement of paws and tail of rats were all evaluated.

Footprint test was used to evaluate the co-ordination of forepaw-hindpaw movements. At day-28 post injury, the paws of rats were painted with different colors (blue for fore-limb and red for hind-limb). The stride length of two hindpaws was analyzed.

Motor-evoked potentials were measured. In brief, rats were anesthetized with a chloral hydrate solution (10%, w/v). The stimulation electrode, recording electrode and reference electrode were applied to the spinal cord rostral ends, the biceps femoris flexor cruris and the distal tendon of the hind limb muscle, respectively. The grounding electrode was placed under the skin. The nerve conduction function of hindlimb was monitored by amplitude under a single square wave stimulus (0.5 mA, 0.5 ms, 1 Hz).

Magnetic resonance imaging

At day 3 post-injury, the level of edema was observed by a magnetic resonance imaging system (Bruker BioSpec 7T/20 USR, Germany). Before imaging, each rat was anesthetized with halothane (3-4% induction, 1.5-2% maintenance) in oxygen (0.4 L/min) and nitrogen (0.6 L/min). After anesthesia, each rat was placed on the fixation system in prone position. The sequence protocol included T2-weighted, 256 × 256 matrix, slice thickness 1 mm, intersection gap 1 mm, echo time (TE)/repetition time (TR) 27/3000 ms, RARE factor 16, and flip angle 90°. A computer-aided software (FireVoxel; CAI2R, New York University, NY) was used for axial images to assess and compare the evolution of

hyperintense signal and lesion volume obtained by adding the individual slice areas and multiplying by 1.0 mm slice plus gap thickness.

Spinal cord tissue immunofluorescence

Spinal cord tissues with lesion segments were collected and fixed in paraformaldehyde (4%, w/v) for 48 h. After dehydrated by sucrose solution (15% and 30%, w/v), spinal cord tissues were cut into 10-mm-thick sections using a cryostat microtome at -30 °C. After blocking by bovine serum albumin (10%, w/v), all spinal sections were incubated with primary antibodies overnight at 4 °C and then with secondary antibodies for 1 hour at room temperature. Primary antibodies used in this study included anti-200 kDa subunit of neurofilament (NF200; mouse; Abcam, UK), anti-glial fibrillary acidic protein (GFAP; rabbit; Abcam, UK), anti-myelin basic protein (MBP; rabbit; CST, USA), and anti-F4/80 (mouse; Santa Cruz Biotechnology, INC., USA). The secondary antibody used was Cy3- or FITC-conjugated secondary antibody (Jackson ImmunoResearch, USA). In addition, 4′,6-diamidino-2-pheny-lindole (DAPI) were used to stain nuclei. Images were taken using a fluorescence microscope (Observe 7, ZEISS, Germany). Volumetric Tissue Exploration and Analysis (VTEA)[37] was employed to qualify the fraction of NF200- positive or F4/80-positive cells.

Statistical analyses

Experiments were performed in at least three independent replicates. Data were processed and analyzed using Origin software (9.7, OriginLab, USA), and presented as the mean ± standard deviation. *P*-values for two-group comparisons and multiple comparisons were calculated using Student's t-test and one-way analysis of variance (ANOVA), respectively.

Acknowledgements

We acknowledge the financial support from the 1000 Youth Talents Plan, Natural Science Foundation of China (No. 81973266 and 51903251), Natural Science Foundation of Jiangsu Province (No. BK20190554) and the Six Talent Peaks Project in Jiangsu Province (No. TD-SWYY-010).

Supporting Information

The supporting Information is available free of charge at http://pubs.acs.org.

Size distribution and stability of MP nanoparticles in dimethyl carbonate; mass ratio of MP and PDA in MP-PLGA@PDA with varied decoration time; the isotherm linear plots and BET plots of MP-PLGA@PDA; cell viabilities of primary neurons incubated with varied concentrations of MP-PLGA@PDA for 72 h; the effect of MP-PLGA@PDA on the level of IL-6, TNF-α and IL-10 under the lipopolysaccharide (LPS) stimulation on glial cells; NF200 positive cells in the distant (>10 mm) field to the lesions plotted from VTEA analysis; the myelin tissue around neuronal axons in the injury site by immunostaining myelin basic protein (MBP).

References

1. Ahuja, C. S.; Wilson, J. R.; Nori, S.; Kotter, M. R. N.; Druschel, C.; Curt, A.; Fehlings, M. G., Traumatic Spinal Cord Injury. *Nat. Rev. Dis. Primers* **2017,** *3* (1), 1-21.

2. Bethea, J. R.; Dietrich, W. D., Targeting the Host Inflammatory Response in Traumatic Spinal Cord Injury. *Curr. Opin. Neurol.* **2002,** *15* (3), 355-360.

3. Allison, D. J.; Ditor, D. S., Immune Dysfunction and Chronic Inflammation Following Spinal Cord Injury. *Spinal Cord* **2015,** *53* (1), 14-18.

4. Ulndreaj, A.; Chio, J. C. T.; Ahuja, C. S.; Fehlings, M. G., Modulating the Immune Response in Spinal Cord Injury. *Expert. Rev. Neurother.* **2016,** *16* (10), 1127-1129.

5. Xu, L. Y.; Botchway, B. O. A.; Zhang, S. G.; Zhou, J. Y.; Liu, X. H., Inhibition of NF-Kappa B Signaling Pathway by Resveratrol Improves Spinal Cord Injury. *Front. Neurosci.* **2018,** *12*, 690.

6. Schomberg, D.; Ahmed, M.; Miranpuri, G.; Olson, J.; Resnick, D. K., Neuropathic Pain: Role of

Inflammation, Immune response, and Ion Channel Activity in Central Injury Mechanisms. *Ann. Neurosci.* **2012,** *19* (3), 125-132.

7. Gao, H. M.; Hong, J. S., Why Neurodegenerative Diseases Are Progressive: Uncontrolled Inflammation Drives Disease Progression. *Trends immunol.* **2008,** *29* (8), 357-365.

8. Chen, P. Y.; Huang, N. T.; Chung, M. T.; Cornell, T. T.; Kurabayashi, K., Label-Free Cytokine Micro- and Nano-Biosensing towards Personalized Medicine of Systemic Inflammatory Disorders. *Adv. Drug Deliv. Rev.* **2015,** *95*, 90-103.

9. Pineau, I.; Lacroix, S., Proinflammatory Cytokine Synthesis in the Injured Mouse Spinal Cord: Multiphasic Expression Pattern and Identification of the Cell Types Involved. *J. Comp. Neurol.* **2007,** *500* (2), 267-285.

10. Bradbury, E. J.; Burnside, E. R., Moving Beyond the Glial Scar for Spinal Cord Repair. *Nat. Commun.* **2019,** *10* (1), 1-15.

11. Mukaino, M.; Nakamura, M.; Yamada, O.; Okada, S.; Morikawa, S.; Renault-Mihara, F.; Iwanami, A.; Ikegami, T.; Ohsugi, Y.; Tsuji, O.; Katoh, H.; Matsuzaki, Y.; Toyama, Y.; Liu, M.; Okano, H., Anti-IL-6-receptor Antibody Promotes Repair of Spinal Cord Injury by Inducing Microglia-dominant Inflammation. *Exp. Neurol.* **2010,** *224* (2), 403-414.

12. Liddelow, S. A.; Guttenplan, K. A.; Clarke, L. E.; Bennett, F. C.; Bohlen, C. J.; Schirmer, L.; Bennett, M. L.; Munch, A. E.; Chung, W. S.; Peterson, T. C.; Wilton, D. K.; Frouin, A.; Napier, B. A.; Panicker, N.; Kumar, M.; Buckwalter, M. S.; Rowitch, D. H.; Dawson, V. L.; Dawson, T. M.; Stevens, B.; Barres, B. A., Neurotoxic Reactive Astrocytes Are Induced by Activated Microglia. *Nature* **2017,** *541* (7638), 481-487.

13. Trivedi, A.; Olivas, A. D.; Noble-Haeusslein, L. J., Inflammation and Spinal Cord Injury: Infiltrating Leukocytes as Determinants of Injury and Repair Processes. *Clin. Neurosci. Res.* **2006,** *6* (5), 283-292.

14. Taoka, Y.; Okajima, K.; Uchiba, M.; Murakami, K.; Kushimoto, S.; Johno, M.; Naruo, M.; Okabe, H.; Takatsuki, K., Role of Neutrophils in Spinal Cord Injury in the Rat. *Neuroscience* **1997,** *79* (4), 1177-1182.

15. Wang, Z.; Duan, Y.; Duan, Y. W., Application of Polydopamine in Tumor Targeted Drug Delivery System and Its Drug Release Behavior. *J. Control. Release* **2018,** *290*, 56-74.

16. Lee, H.; Dellatore, S. M.; Miller, W. M.; Messersmith, P. B., Mussel-Inspired Surface Chemistry for Multifunctional Coatings. *Science* **2007,** *318* (5849), 426-430.

17. Jeong, K. J.; Wang, L. Q.; Stefanescu, C. F.; Lawlor, M. W.; Polat, J.; Dohlman, C. H.; Langer, R. S.; Kohane, D. S., Polydopamine Coatings Enhance Biointegration of a Model Polymeric Implant. *Soft Matter* **2011,** *7* (18), 8305-8312.

18. Bracken, M. B.; Shepard, M. J.; Collins, W. F.; Holford, T. R.; Baskin, D. S.; Eisenberg, H. M.; Flamm, E.; Leosummers, L.; Maroon, J. C.; Marshall, L. F.; Perot, P. L.; Piepmeier, J.; Sonntag, V. K. H.; Wagner, F. C.; Wilberger, J. L.; Winn, H. R.; Young, W., Methylprednisolone or Naloxone Treatment after Acute Spinal-Cord Injury: 1-Year Follow-up Data - Results of the 2nd National Acute Spinal-Cord Injury Study. *J. Neurosurg.* **1992,** *76* (1), 23-31.

19. Barnes, P. J., Anti-inflammatory Actions of Glucocorticoids: Molecular Mechanisms. *Clin. Sci.* **1998,** *94* (6), 557-572.

20. Utada, A. S.; Chu, L. Y.; Fernandez-Nieves, A.; Link, D. R.; Holtze, C.; Weitz, D. A., Dripping, Jetting, Drops, and Wetting: The Magic of Microfluidics. *MRS Bulletin* **2007,** *32* (9), 702-708.

21. Dreyer, D. R.; Miller, D. J.; Freeman, B. D.; Paul, D. R.; Bielawski, C. W., Elucidating the Structure of Poly(dopamine). *Langmuir* **2012,** *28* (15), 6428-6435.

22. Brunauer, S.; Deming, L. S.; Deming, W. E.; Teller, E., On a Theory of the Van Der Waals Adsorption of Gases. *J. Am. Chem. Soc.* **1940,** *62* (7), 1723-1732.

23. Gal, P.; Kravcukova, P.; Mokry, M.; Kluchova, D., Chemokines as Possible Targets in Modulation of the Secondary Damage after Acute Spinal Cord Injury: A Review. *Cell. Mol. Neurobiol.* **2009,** *29* (6-7), 1025-1035.

24. Esposito, E.; Cuzzocrea, S., Anti-TNF Therapy in the Injured Spinal Cord. *Trends Pharmacol. Sci.* **2011,** *32* (2), 107-115.

25. Lacroix, S.; Chang, L.; Rose-John, S.; Tuszynski, M. H., Delivery of Hyper-Interleukin-6 to the Injured Spinal Cord Increases Neutrophil and Macrophage Infiltration and Inhibits Axonal Growth. *J. Comp. Neurol.* **2002,** *454* (3), 213-228.

26. Thompson, C. D.; Zurko, J. C.; Hanna, B. F.; Hellenbrand, D. J.; Hanna, A., The Therapeutic Role of Interleukin-10 after Spinal Cord Injury. *J. Neurotrauma* **2013,** *30* (15), 1311-1324.

27. Jia, M. D.; Deng, C. F.; Luo, J. W.; Zhang, P.; Sun, X.; Zhang, Z. R.; Gong, T., A Novel Dexamethasone-Loaded Liposome Alleviates Rheumatoid Arthritis in Rats. *Int. J. Pharm.* **2018,** *540* (1-2), 57-64.

28. Wan, T.; Li, L. L.; Guo, M.; Jiao, Z. X.; Wang, Z. L.; Ito, Y.; Wan, Y. Z.; Zhang, P. B.; Liu, Q. Y., Immobilization via Polydopamine of Dual Growth Factors on Polyetheretherketone: Improvement of Cell Adhesion, Proliferation, and Osteo-differentiation. *J. Mater. Sci.* **2019,** *54* (16), 11179-11196.

29. Wang, Y. L.; Qi, H. N.; Miron, R. J.; Zhang, Y. F., Modulating Macrophage Polarization on Titanium Implant Surface by Poly(dopamine)-Assisted Immobilization of IL4. *Clin. Implant Dent. Res.* **2019,** *21* (5), 977-986.

30. Li, M. T.; Wei, F.; Yin, X. Q.; Xiao, L.; Yang, L.; Su, J. H.; Weng, J.; Feng, B.; Xiao, Y.; Zhou, Y. H., Synergistic Regulation of Osteoimmune Microenvironment by IL-4 and RGD to Accelerate

Osteogenesis. *Mater. Sci. Eng. C* **2020,** *109*, No. 110805.

31. Lee, Y. B.; Shin, Y. M.; Lee, J. H.; Jun, I.; Kang, J. K.; Park, J. C.; Shin, H., Polydopamine-Mediated Immobilization of Multiple Bioactive Molecules for the Development of Functional Vascular Graft Materials. *Biomaterials* **2012,** *33* (33), 8343-8352.

32. Barclay, T. G.; Hegab, H. M.; Clarke, S. R.; Ginic-Markovic, M., Versatile Surface Modification Using Polydopamine and Related Polycatecholamines: Chemistry, Structure, and Applications. *Adv. Mater. Interfaces* **2017,** *4* (19), No. 1601192.

33. Chen, C. T.; Buehler, M. J., Polydopamine and Eumelanin Models in Various Oxidation States. *Phys. Chem. Chem. Phys.* **2018,** *20* (44), 28135-28143.

34. David, S.; Kroner, A., Repertoire of Microglial and Macrophage Responses after Spinal Cord Injury. *Nat. Rev. Neurosci.* **2011,** *12* (7), 388-399.

35. Gao, H. M.; Hong, J. S., Why Neurodegenerative Diseases Are Progressive: Uncontrolled Inflammation Drives Disease Progression. *Trends Immunol.* **2008,** *29* (8), 357-365.

36. Hara, M.; Kobayakawa, K.; Ohkawa, Y.; Kumamaru, H.; Yokota, K.; Saito, T.; Kijima, K.; Yoshizaki, S.; Harimaya, K.; Nakashima, Y.; Okada, S., Interaction of Reactive Astrocytes with Type I Collagen Induces Astrocytic Scar Formation through the Integrin-N-Cadherin Pathway after Spinal Cord Injury. *Nat. Med.* **2017**, *23* (7), 818-828.

37. Winfree, S.; Khan, S.; Micanovic, R.; Eadon, M. T.; Kelly, K. J.; Sutton, T. A.; Phillips, C. L.; Dunn, K. W.; El-Achkar, T. M., Quantitative Three-Dimensional Tissue Cytometry to Study Kidney Tissue and Resident Immune Cells. *J. Am. Soc. Nephrol.* **2017,** *28* (7), 2108-2118.

38. Petzold, A., Neurofilament Phosphoforms: Surrogate Markers for Axonal Injury, Degeneration and Loss. *J. Neurol. Sci.* **2005,** *233* (1-2), 183-198.

39. Liu, D.; Bernuz, C. R.; Fan, J.; Li, W.; Correia, A.; Hirvonen, J. T.; Santos, H. A., A Nano-in-Nano Vector: Merging the Best of Both Polymeric Nanoparticles and Drug Nanocrystals. *Adv. Funct. Mater.* **2017,** *27*, No. 1604508.

40. Lin, L. S.; Cong, Z. X.; Cao, J. B.; Ke, K. M.; Peng, Q. L.; Gao, J. H.; Yang, H. H.; Liu, G.; Chen, X. Y., Multifunctional Fe3O4@Polydopamine Core-Shell Nanocomposites for Intracellular mRNA Detection and Imaging-Guided Photothermal Therapy. *ACS Nano* **2014,** *8* (4), 3876-3883.

41. Brunauer, S.; Emmett, P. H.; Teller, E., Adsorption of Gases in Multimolecular Layers. *J. Am. Chem. Soc.* **1938,** *60* (2), 309-319.

42. Schildge, S.; Bohrer, C.; Beck, K.; Schachtrup, C., Isolation and Culture of Mouse Cortical Astrocytes. *Jove-J Vis. Exp.* **2013,** *71*, No. 50079.

43. Chen, W. F.; Chen, C. H.; Chen, N. F.; Sung, C. S.; Wen, Z. H., Neuroprotective Effects of Direct Intrathecal Administration of Granulocyte Colony-Stimulating Factor in Rats with Spinal Cord Injury.

CNS Neurosci. Ther. **2015,** *21* (9), 698-707.

44. Mahat, M. Y.; Fakrudeen Ali Ahamed, N.; Chandrasekaran, S.; Rajagopal, S.; Narayanan, S.; Surendran, N., An Improved Method of Transcutaneous Cisterna Magna Puncture for Cerebrospinal Fluid Sampling in Rats. *J. Neurosci. Methods* **2012,** *211* (2), 272-279.

45. Ceaglio, N.; Orozco, G.; Etcheverrigaray, M.; Mattio, M.; Kratje, R.; Perotti, N.; Oggero, M., High Performance Collection of Cerebrospinal Fluid in Rats: Evaluation of Erythropoietin Penetration after Osmotic Opening of the Blood-Brain Barrier. *J. Neurosci. Methods* **2013,** *219* (1), 70-75.

For Table of Contents Only

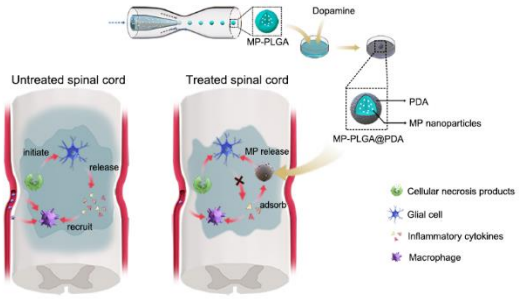

Supporting Information

Polydopamine-decorated Microcomposites Promote Functional Recovery of Injured Spinal Cord by Inhibiting Neuroinflammation

Guangfei Wei[a, b§], Dongdong Jiang[c§], Shuai Hu[a, b], Zhiyuan Yang[a, b], Zifan Zhang[a, b], Wei Li[d], Weihua Cai[c*], Dongfei Liu[a, b*]

[a] *State Key Laboratory of Natural Medicines, Department of Pharmaceutical Science, China Pharmaceutical University, Nanjing 210009, China*

[b] *NMPA Key Laboratory for Research and Evaluation of Pharmaceutical Preparations and Excipients, China Pharmaceutical University, Nanjing 210009, China*

[c] *Department of Orthopaedics, The First Affiliated Hospital of Nanjing Medical University, Nanjing 210029, China*

[d] *Drug Research Program, Division of Pharmaceutical Chemistry and Technology, Faculty of Pharmacy, University of Helsinki, Helsinki 00014, Finland*

* E-mail: dongfei.liu@cpu.edu.cn

* E-mail: caiwhspine@sina.com

§ *Guangfei Wei and Dongdong Jiang contributed equally to this paper*

* *Weihua Cai and Dongfei Liu are the corresponding authors of this paper*

Stability of MP nanoparticles

MP nanoparticles in dimethyl carbonate solution were obtained using ball milling method (Emax, Retsch, Germany). These MP nanoparticles had an average diameter of 237 nm with a polydispersity index of 0.14, which could be stably dispersed in dimethyl carbonate for at least 12 h (**Fig S1**).

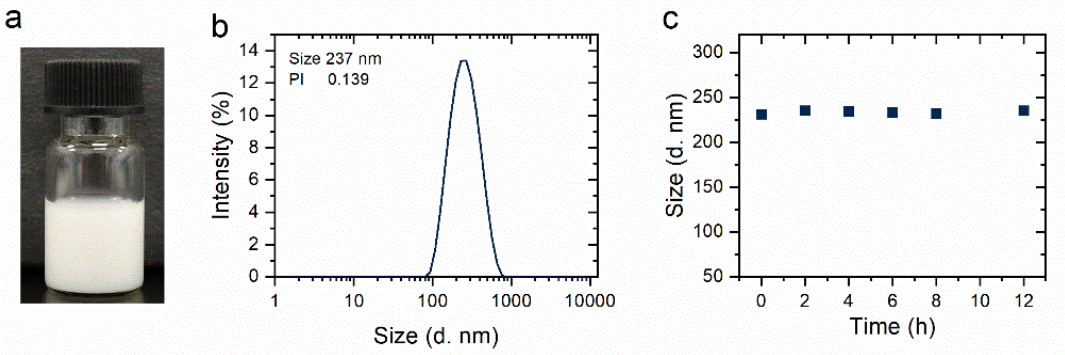

Fig S1. Appearance (**a**) and size distribution (**b**) of MP nanoparticles in dimethyl carbonate prepared by ball milling method. The size stability (**c**) of MP nanoparticles in dimethyl carbonate at room temperature.

Loading degree of MP and mass ratio of PDA in MP-PLGA@PDA

Drug loading of microspheres was expressed as [(weight of loaded drug/weight of drug loaded samples) × 100%]. After preparation, the MP loading degree in MP-PLGA was 55.8 ± 0.2%, shown in **Fig S2**. However, the MP loading declined from approximately 55.8% to approximately 39.9% after 24 h incubation in a dopamine hydrochloride solution (**Fig S2**a). To confirm whether MP leaked from microspheres during the PDA decoration process, MP-PLGA was immersed in Tris-HCl (10 mM, pH 8.5, without dopamine hydrochloride) for 24 hours. At the given time, these immersed MP-PLGA were withdrawn to analyze MP content in them. After immersion for 24 h, MP loading of MP-PLGA did not decrease significantly (compared with the initial MP loading degree, 55.8 ± 0.2%, $p > 0.05$), which was 53.4 ± 0.3% (**Fig S2**b), indicating 24 h incubation of MP-PLGA in Tris-HCl (10 mM, pH 8.5) had no effects on MP loading.

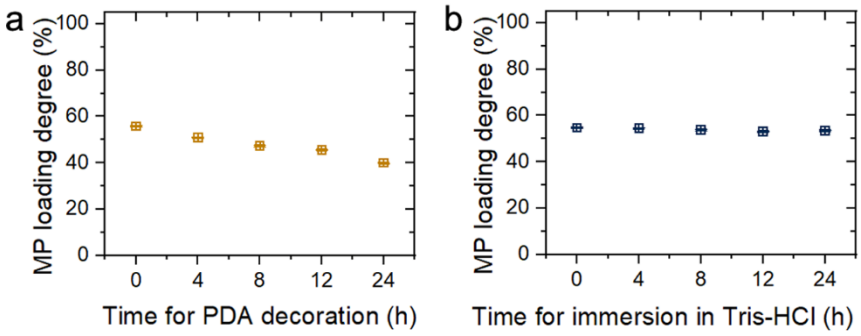

Fig S2. MP loading degree of MP-PLGA after immersing in dopamine hydrochloride Tris-HCl solution (a) or Tris-HCl (b) for 0, 4, 8, 12 and 24 h (n = 3).

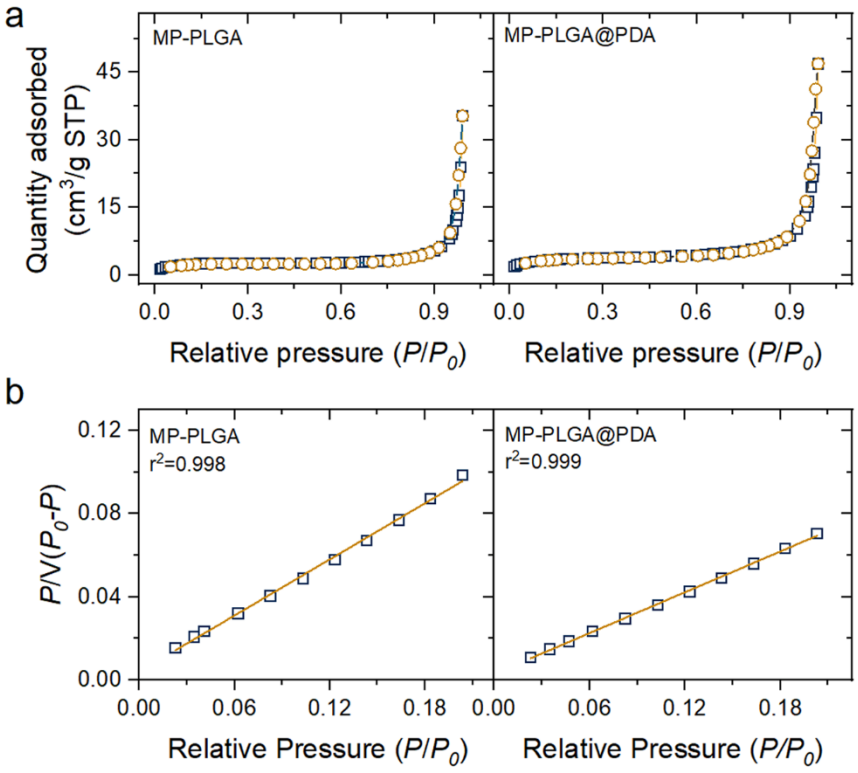

Fig S3. The isotherm linear plots (a) and BET plots for nitrogen adsorption (b) of MP-PLGA and MP-PLGA@PDA, which were obtained by nitrogen adsorption-desorption method.

Cytotoxicity studies

We evaluated the cytocompatibility of MP-PLGA@PDA on primary neurons obtained from rat hippocampal neurons according to a standard protocol[1, 2]. The primary neurons were cultured in 96-

well plates at a density of 1 x 10^4 per well and incubated for 24 h. After 72 h incubation with different concentrations of MP-PLGA@PDA (31.25-500 μg/mL), the cells were washed with PBS, and then assessed by Cell Counting Kit-8 (CCK-8, Dojindo, Kumamoto, Japan). The living cells were identified at 450 nm by an absorbance microplate reader (ELx800, Bio-Tek, USA). Then, cell viability was calculated according to the following equation: (T-B)/(C-B) × 100%, where T is the absorbance of the treatment group; C is the absorbance of the untreated (control) group; B refers to the absorption value of the culture medium. As depicted in **Fig S4**, no obvious cytotoxicity was observed for MP-PLGA@PDA within the tested concentration range (31.25-500 μg/mL). The cell viabilities for MP-PLGA@PDA (90.8% ± 4.2%) at a high dose (500 μg/mL) was not significantly different from that for the control group (93.3% ± 4.8%), revealing the good biocompatibility of MP-PLGA@PDA with neurons.

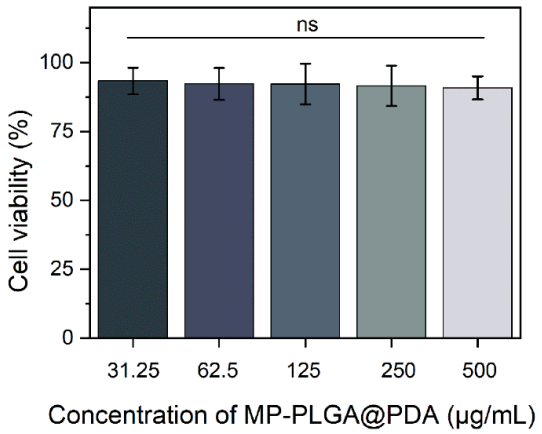

Fig S4. Cell viabilities of primary neurons incubated with varied concentrations of MP-PLGA@PDA for 72 h (*n*=5). ns, not significant.

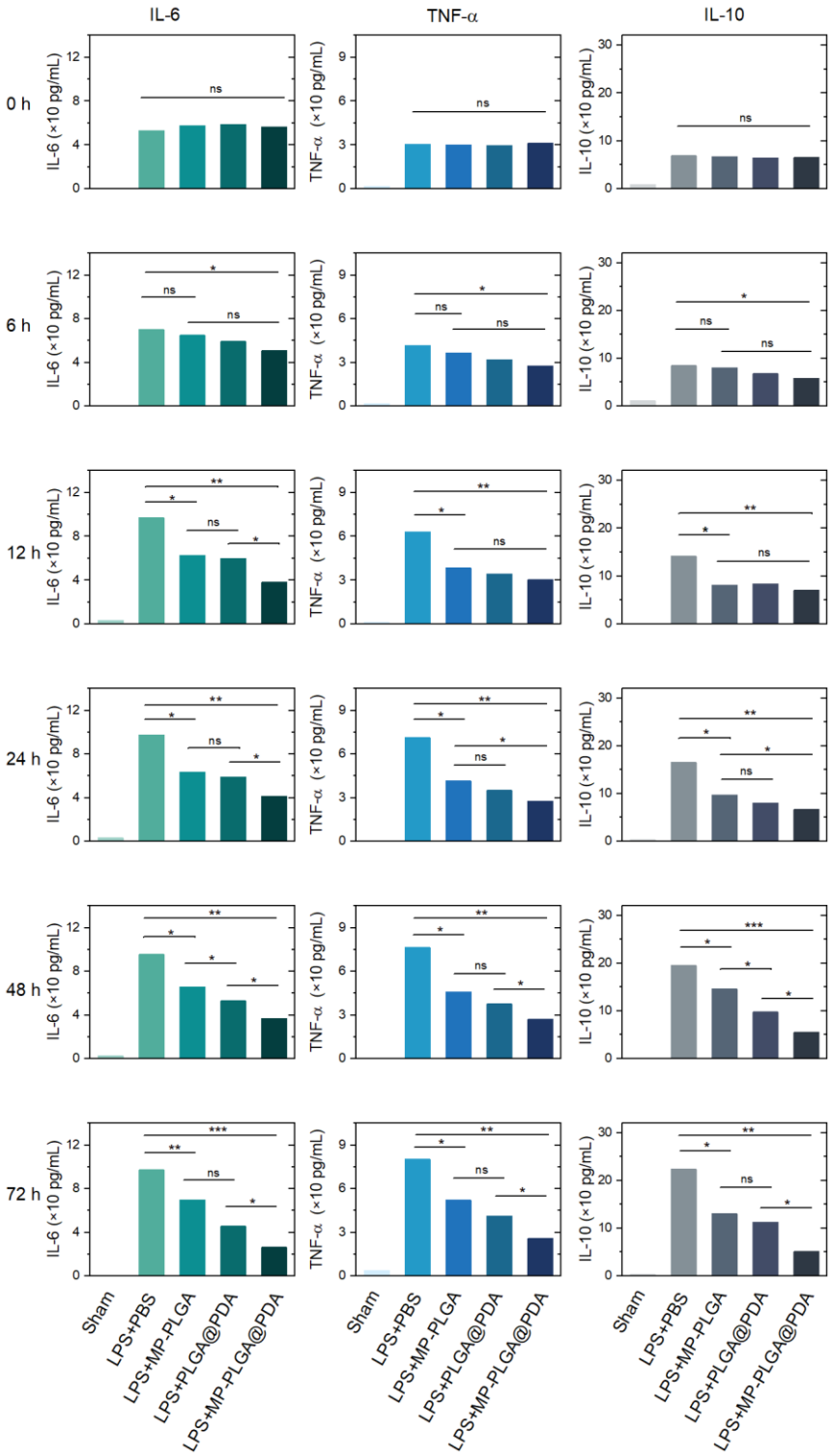

Fig S5. The effect of MP-PLGA@PDA on the level of IL-6, TNF-α and IL-10 under the lipopolysaccharide (LPS) stimulation on glial cells for 72 h (n = 6). ns, not significant; $^{*}P < 0.05$; $^{**}P < 0.01$; $^{***}P < 0.001$.

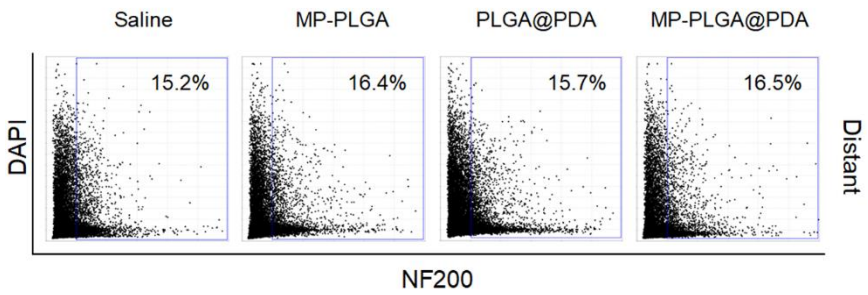

Fig S6. NF200 positive cells in regions located >10 mm from the border of the injury at day 28 post-injury. Cells were identified, and their average DAPI versus the average NF200 intensity was plotted from VTEA analysis. A gate was drawn identifying cells with high NF200 immunofluorescence.

MP-PLGA@PDA protected neurons

Myelin basic protein (MBP) is the main marker that wraps the myelin tissue of neuronal axons and is highly expressed in the white matter of spinal cord[3]. We evaluated the myelin tissue around neuronal axons in the injury site by immunostaining MBP (in green, rabbit; CST, USA) to further verify the neuroprotection of MP-PLGA@PDA (**Fig S7**). Neuronal axons were immunostained by the 200kDa subunit of a neurofilament (NF200, in red, mouse; Abcam, UK). The intensity decrease was calculated based on the MBP intensity in regions near lesion and that in remote regions (located >10 mm from the border of the injury). At day 28 post-injury, Saline group had a disordered MBP staining near the peritraumatic area with a 37.5 ± 6.2% decrease in MBP intensity. In comparison with Saline group, the decrease of MBP intensity was significantly reduced ($P < 0.05$) to 26.2 ± 3.5%, 25 ± 3.8% and 10.5 ± 4.6% for MP-PLGA, PLGA@PDA and MP-PLGA@PDA, respectively. Moreover, we observed MBP-wrapped axons (MBP positive and NF200 positive area) growing into the injured area in the MP-PLGA@PDA group. These results suggested that MP-PLGA@PDA could inhibit the demyelination changes in the injured area, and protect the neurons in the injury site.

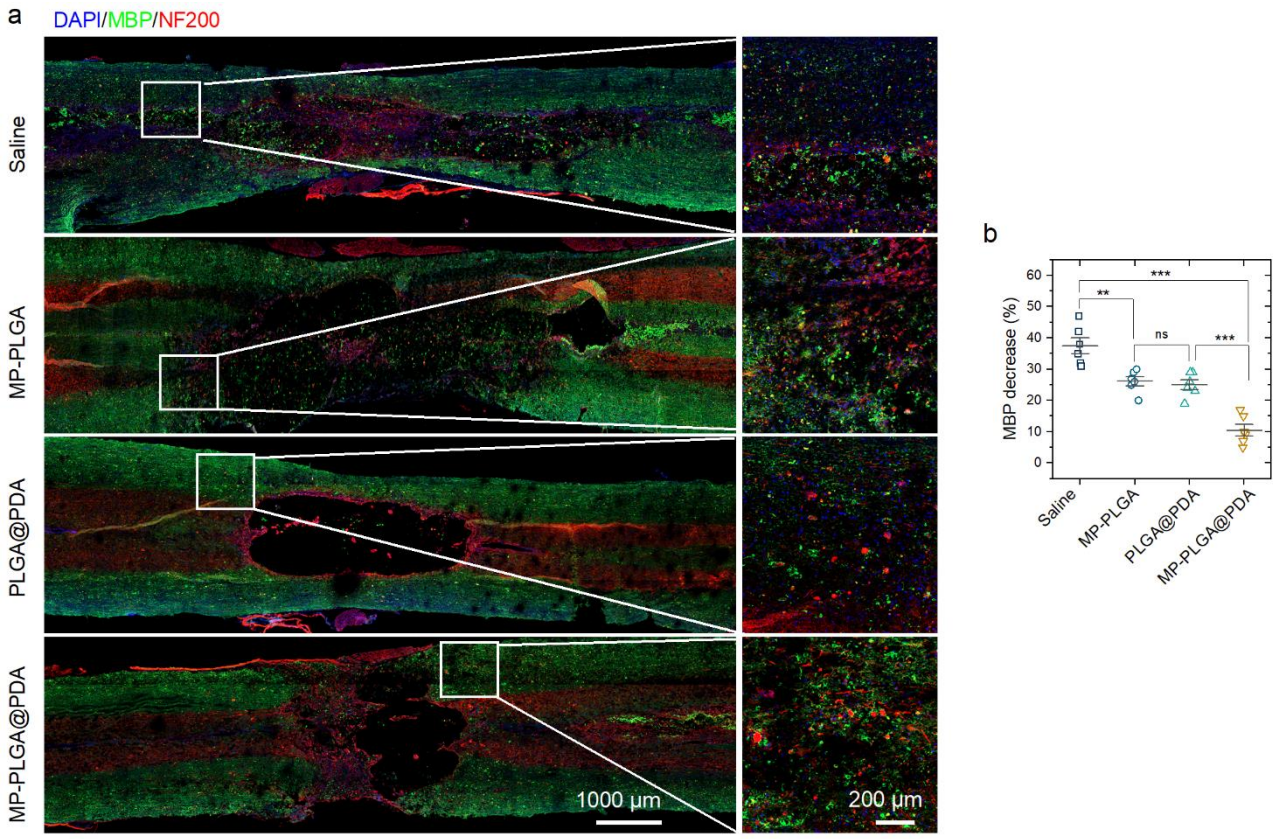

Fig S7. (**a**) Immunofluorescence staining of MBP (in green) and NF200 (in red) in injured spinal cord at day-28 post trauma. The right columns are the enlarged images corresponding to the area adjacent to the lesion. (**b**) Semi-quantification the effect of MP-PLGA@PDA on the intensity decreases of MBP. The data are plotted as the relative value of MBP intensity near the injury site compared with that in distant area (n = 6). ns, not significant; $^{**}P < 0.01$; $^{***}P < 0.001$.

References

1. Periyasamy, P.; Liao, K.; Kook, Y. H.; Niu, F.; Callen, S. E.; Guo, M. L.; Buch, S., Cocaine-Mediated Downregulation of miR-124 Activates Microglia by Targeting KLF4 and TLR4 Signaling. *Mol. Neurobiol.* **2018,** *55* (4), 3196-3210.

2. Ni, M.; Aschner, M., Neonatal Rat Primary Microglia: Isolation, Culturing, and Selected Applications. *Curr. Protoc. Toxicol.* **2010,** *Chapter 12*, Unit 12-17.

3. Hauben, E.; Butovsky, O.; Nevo, U.; Yoles, E.; Moalem, G.; Agranov, E.; Mor, F.; Leibowitz-Amit, R.; Pevsner, E.; Akselrod, S.; Neeman, M.; Cohen, I. R.; Schwartz, M., Passive or Active Immunization with Myelin Basic Protein Promotes Recovery from Spinal Cord Contusion. *J. Neurosci.* **2000,** *20* (17), 6421-6430.